ISSN 0023-1584, Kinetics and Catalysis, 2023, Vol. 64, No. 4, pp. 449–457. © Pleiades Publishing, Ltd., 2023.
Russian Text © The Author(s), 2023, published in Kinetika i Kataliz, 2023, Vol. 64, No. 4, pp. 447–456.

Ceria–Zirconia Supported Platinum Catalysts for the Water-Gas Shift Reaction: The Influence of Support Composition

A. M. Gorlova[a, b, *], V. P. Pakharukova[a, b], O. A. Stonkus[a, b], V. N. Rogozhnikov[a], A. Y. Gladky[a], P. V. Snytnikov[a], and D. I. Potemkin[a, b]

[a] *Boreskov Institute of Catalysis, Novosibirsk, 630090 Russia*
[b] *Novosibirsk State University, Novosibirsk, 630090 Russia*
**e-mail: gorlova@catalysis.ru*

Received December 19, 2022; revised March 6, 2023; accepted March 15, 2023

Abstract—The study is presented on the influence of the composition of a ceria-zirconia support on the structure and the activity in water-gas shift reaction of platinum catalysts ($Pt/Ce_{0.75}Zr_{0.25}O_2$ and $Pt/Ce_{0.4}Zr_{0.5}Y_{0.05}La_{0.05}O_2$). The structure diagnostics of the samples were performed using high-resolution transmission electron microscopy, powder X-ray diffraction, CO chemisorption and X-ray atomic pair distribution function method. It was shown that the catalysts contain highly dispersed platinum particles not exceeding 2 nm in size. Platinum particles supported on $Ce_{0.75}Zr_{0.25}O_2$ are smaller due to the higher specific surface area of the support. The catalysts $Pt/Ce_{0.75}Zr_{0.25}O_2$ and $Pt/Ce_{0.4}Zr_{0.5}Y_{0.05}La_{0.05}O_2$ proved to have similar efficiency while having the same platinum content. It was assumed that the catalysts supported on $Ce_{0.4}Zr_{0.5}Y_{0.05}La_{0.05}O_2$ demonstrate a slightly higher turnover frequency per platinum surface atom, but it is likely compensated by the difference in the supported metal particle size.

Keywords: water-gas shift, hydrogen purification, platinum catalyst, ceria-zirconia

DOI: 10.1134/S0023158423040031

INTRODUCTION

Pure hydrogen production is one of the key problem for hydrogen economy. Hydrogen generation from water requires minimum efforts for purifying and separation of the gas mixture and is considered to be the best choice, although not being economically and ecologically viable in most cases. Therefore, the studies of the processes of hydrogen production from syngas are of high importance. In its turn, syngas can be obtained from the variety of organics [1, 2]. In this case, total CO removal from the hydrogen-rich gas is essential, since this impurity poisons, specifically, the platinum electrocatalysts in the proton-exchange membrane fuel cells, and its content in hydrogen must not exceed 10 ppm [3]. To meet this target, a two-step purification process is considered. The first stage—water-gas shift reaction (WGS)—provides for the oxidation of most of CO to CO_2 which can be easily adsorbed and separated from hydrogen. Then CO residual (~1%) can be oxidized to CO_2 by oxygen [4] or reduced to CH_4 [5].

Over the last decades catalytic systems based on CeO_2 have been considered to be one of the best alternatives to Cu-Zn oxide catalysts used for industrial WGS implementation [6, 7]. In particular, the former do not require the long-time preliminary activation and are tolerant of oxygen traces, and it favorably distinguishes them from the latter ones [7]. Deposition of the noble metals (Pt, Au) on CeO_2 makes it possible to obtain the catalysts providing for the highly effective WGS process at relatively low temperatures [8, 9]. It is of particular importance to decrease the temperature of WGS, because higher temperatures lead to lower CO conversion [10]. For this reason, the catalyst active at lower temperatures can potentially provide for required CO concentration in one stage.

The effectiveness of CeO_2-based catalysts in WGS is caused by their strong interaction with the supported metal, as well as by the high oxygen mobility and facile Ce^{3+}–Ce^{4+} transition which allows for the formation of a large quantity of oxygen vacancies [11, 12]. Despite of the lack of information on the nature of the active sites in CeO_2-based catalysts, there is an increase in a number of studies confirming a hypothesis on the localization of the reaction on the metal-

Abbreviations and notation: WGS, water gas shift; WHSV, weight hourly space velocity; ICP-AES, inductively coupled plasma-atomic emission spectroscopy; XRD, X-ray diffraction; CSR, coherent scattering region; PDF, pair distribution function analysis; HR TEM, high-resolution transmission electron microscopy; TPR, temperature-programmed reduction; TPD, temperature-programmed reduction; S_{BET}, specific surface area; V_{pore}, total pore volume; $V_{micropore}$, micropore volume.

support interface: CO is adsorbed on Pt atom, while H_2O adsorption and dissociation take place on an oxygen vacancy [13–15]. This way, the number of oxygen vacancies on the surface of the oxide can be one of the factors affecting the activity of a catalyst in WGS.

Despite the described advantages, CeO_2 also has some limitations. For example, this oxide undergoes sintering at high temperatures and has poor mechanical stability [16, 17], which is important in the case of pelleted catalysts. Doping the oxide with zirconium was suggested to improve these characteristics [17]. It was shown [18–22] that $Ce_{1-x}Zr_xO_2$ demonstrates better thermal stability and oxygen mobility, as well as facilitates the formation of larger amount of oxygen vacancies on the surface of the oxide providing for better performance of the catalyst. At the same time, there is a possibility of the formation of the ZrO_2 phase at $x \geq 0.45$, which can lead to the blocking of the contact between CeO_2 and metal and, hence, degrade the activity [20]. Apart from Zr, La [23–28], Y [25, 29, 30], Gd [24, 28, 31], Sm [26, 30, 32], Pr [33–35] and other rare-earth and transition metals are used as dopants to increase the number of the defects in the structure of the oxide.

In this work, the study is presented on the influence of the ceria-zirconia composition on the structure of the supported platinum catalysts. Two oxide supports $Ce_{0.75}Zr_{0.25}O_2$ and $Ce_{0.4}Zr_{0.5}Y_{0.05}La_{0.05}O_2$ were taken for this purpose. The correlation was analyzed between the textural characteristics of the support, the supported Pt particle size and the catalytic activity of the obtained samples in WGS in the reformate-simulating feed gas.

MATERIALS AND METHODS

Catalyst Preparation

The oxide support $Ce_{0.75}Zr_{0.25}O_2$ (denoted as CeZr) was synthesized by the coprecipitation technique. $Ce(NO_3)_3 \cdot 6H_2O$ and $ZrO(NO_3)_2 \cdot 8H_2O$ were used as precursors for ceria and zirconia. Ammonia aqueous solution was used as precipitator. To synthesize $Ce_{0.75}Zr_{0.25}O_2$ support, nitrates were mixed in mole ratio Ce : Zr = 3 : 1 and dissolved in water under stirring until a transparent solution was obtained. Cerium and zirconium hydroxides were coprecipitated by the reverse precipitation method, i.e. the aqueous solution of cerium and zirconyl nitrates was added dropwise to the ammonia aqueous solution. After that the resulted precipitate was aged for 30 min and then filtrated. It was dried at 80°C for 15 h and calcined at 450°C. Also commercial (Optalys ®) oxide support $Ce_{0.4}Zr_{0.5}Y_{0.05}La_{0.05}O_2$ (CeZrYLa) was used for catalyst preparation. Both the supports have packed density of ~0.4 g/cm^3.

1.9 and 5 wt % of platinum was deposited on the supports by the sorption-hydrolytic technique [36, 37]. A portion of K_2PtCl_4 was dissolved in distilled water in a thermostatic beaker, then a portion of the oxide powder was added. Na_2CO_3 solution was added dropwise under stirring with a magnetic stirrer (~0.05 M, Na_2CO_3 : K_2PtCl_4 = 1.1 : 1). After that the slurry was being mixed at 25°C for 15 min, then—at 80°C for 40 min. After this time was over, the solution was checked for the presence of Pt ions using $NaBH_4$—ones have not been detected, and for this reason all the platinum was supposed to be deposited on the surface of the support (which was confirmed later by the analysis of the prepared catalysts using ICP-AES). The solution was separated from the solid phase which was then washed with ~100 mL of hot water and dried for 9 h in a desiccator at 80°C. The sample was reduced in H_2 flow at 350°C for 1 h.

Catalytic Tests

The catalytic tests of the prepared samples in WGS were carried out in a glass tubular U-shaped flow reactor (inner diameter 3 mm). The catalyst load was 125 mg, 0.2-0.5 mm fraction, WHSV was 30000 mL g_{cat}^{-1} h^{-1}. The composition of the feed gas (vol %): 10 CO, 15 CO_2, 45 H_2, 30 H_2O (with an accuracy of ±1 abs. %). The temperature of the catalyst bed was controlled using K-type thermocouple placed right in its center. Water vapour was supplied using a saturator which provided for its stable concentration in the feed gas during the experiments (the gas pipes were heated before and after the reactor). The gas mixture before and after the reactor was analyzed using a gas chromatograph Chromos GC-1000 (Chromos, Russia) equipped with a thermal conductivity detector (CaA molecular sieves column) and flame-ionization detector (PorapakQ column) with a methanator, the sensitivity to CO, CO_2 and CH_4 concentrations was about 1 ppm. The separation of C-containing compounds on the column with a subsequent methanation of carbon oxides allows analyzing them using flame-ionization detector with an accuracy of ±3 rel %.

Catalyst Characterization

The textural characteristics (specific surface area (S_{BET}), total pore volume (V_{pore}) and micropore volume ($V_{micropore}$)) of the oxide supports and the catalysts based on them were studied by the low-temperature N_2 adsorption at −196°C using a surface area analyzer ASAP 2400 (Micromeritics Instrument Corporation, USA).

X-ray diffraction analysis (XRD) was carried out at transmission mode using the MoK_α-radiation (λ = 0.7093 Å) by means of a STADI MP diffractometer (STOE, Germany) equipped with a MYTHEN2 1K detector (Dectris AG, Switzerland). The measurements were performed in the 2θ range from 1° to 137°

with an interval of 0.015°. The average scatter coherent region size (CSR) of the detected phases were calculated from the peak broadenings using Scherrer equation. An instrumental broadening, which was determined from the XRD pattern of a standard sample NIST SRM 660c (LaB_6), was also taken into account.

For the structural diagnostics of the highly dispersed platinum compounds in the catalysts on the atomic level atomic pair distribution function analysis (PDF) was used [38–40]. The atomic pair distribution function, $G(r)$, shows the distribution of the interatomic distances in the material under study. The coordination peak positions correspond to the equilibrium interatomic distances, the peak areas are related to abundance of the corresponding atomic pair (coordination number) and scattering ability of the atoms.

$G(r)$ function is calculated using Fourier transformation of the reduced total scattering function:

$$G(r) = \frac{2}{\pi}\int_0^\infty Q\mathrm{i}(Q)\sin(Qr)dQ, \quad (1)$$

where $Q = (4\pi\sin\theta)/\lambda$ is the scattering vector value; λ—the radiation wavelength; $\mathrm{i}(Q)$ is interference part of scattering intensity.

The main stages of the data processing include corrections for the background, absorption, exclusion of the contribution of incoherent Compton scattering, separation of the interference part of the scattering intensity due to the ordered arrangement of atoms [38]. The $G(r)$ function resolution depends on the maximum scattering vector value Q_{max}. The experimental data obtained in this work correspond to the value $Q_{max} = 15.8$ Å^{-1}. $G(r)$ function calculation was performed using PDFgetX2 software [41]. The calculation of the model $G(r)$ functions was carried out using PDFfit2 software [42] based on the structural data presented in the ICSD database [43]. The corrections dealt with a small size of the model particles were made using spherical shape factor "cutting" the $G(r)$ function [44, 45].

The study of the samples was performed by means of transmission electron microscopes (TEM) JEM-2010 and JEM-2200FS (JEOL, Japan) with the resolution of 1.4 and 1 Å, respectively, operated at 200 kV. The samples were prepared on a perforated carbon film mounted on a copper grid of 3 mm mesh. Alcoholic suspensions were dispersed by ultrasonication and deposited onto the substrates.

CO chemisorption studies of the samples were performed using TPR/TPD analyzer ChemBET Pulsar (Quantachrome Inst., USA). For each experiment 0.05 g of the sample were placed into the quartz tube, heated in 10% H_2/He flow to 250°C with the heating rate of 10°C/min and kept at this temperature for 25 min, total reduction of the samples was determined from the observed hydrogen uptake. Then the samples were cooled in He flow to 30°C, and pulse titration by the mixture 10% CO in He was performed. After that the samples were oxidized by air at room temperature for 30 min, and the cycle was repeated. Specific surface area and particle size of Pt were calculated from the obtained data given the assumptions: 1) one CO molecule is adsorbed on one metal atom; 2) the particles are spherical.

Table 1. Textural characteristics of the supports and the as-prepared catalysts containing 5 wt % Pt*

Sample	S_{BET}, m^2/g	V_{pore}, cm^3/g	$V_{micropore}$, cm^3/g
CeZr	80	0.20	0
CeZrYLa	73	0.35	0
5% Pt/CeZr	78	0.18	0
5% Pt/CeZrYLa	70	0.31	0

* The accuracy of S_{BET}, V_{pore} and $V_{micropore}$ estimation is 10 rel %.

RESULTS AND DISCUSSION

The textural characteristics of the as-prepared samples containing 5 wt % Pt, as well as pure supports were studied by low-temperature nitrogen adsorption (Table 1). With an error of S_{BET} estimation of about 10 rel % taken into account, one can conclude that Pt deposition did not lead to significant changes in the specific surface area and did not cause blocking of the transport pores.

Catalytic tests of the samples in WGS using reformate-simulating feed gas showed that, as long as the platinum loadings are the same, there is no noticeable influence of the support on the process effectiveness (Fig. 1a). With regard to the side reaction of methanation of carbon oxides, which can occur under these conditions, no significant differences were found either (Fig. 1b).

It should be noted that an increase of platinum loading influences positively on the temperature of the highest CO conversion. For example, in the case of the catalysts with 5 wt % Pt the minimum of CO concentration was observed at $T \approx 280$°C, while for 1.9 wt % Pt—only at $T \approx 310$°C. Performing the WGS process at lower temperatures is more favorable not only for higher CO to CO_2 conversion. It is seen from the Fig. 1b that at $T < 280$°C the contribution of the side reaction of methanation is negligible which allows obtaining hydrogen of higher purity after the reaction.

Platinum catalysts containing 5 wt % Pt before and after WGS, as well as pure oxide supports were investigated by means of XRD (Fig. 2). According to the obtained data, the CeZr support ($Ce_{0.75}Zr_{0.25}O_2$) represent single phase of a substitution solid solution with a cubic fluorite-type structure (space group $Fm\bar{3}m$) (Fig. 2a). The value of the cubic cell parameter a of the mixed oxide $Ce_{1-x}Zr_xO_2$ is 5.352(1) Å. The ratio

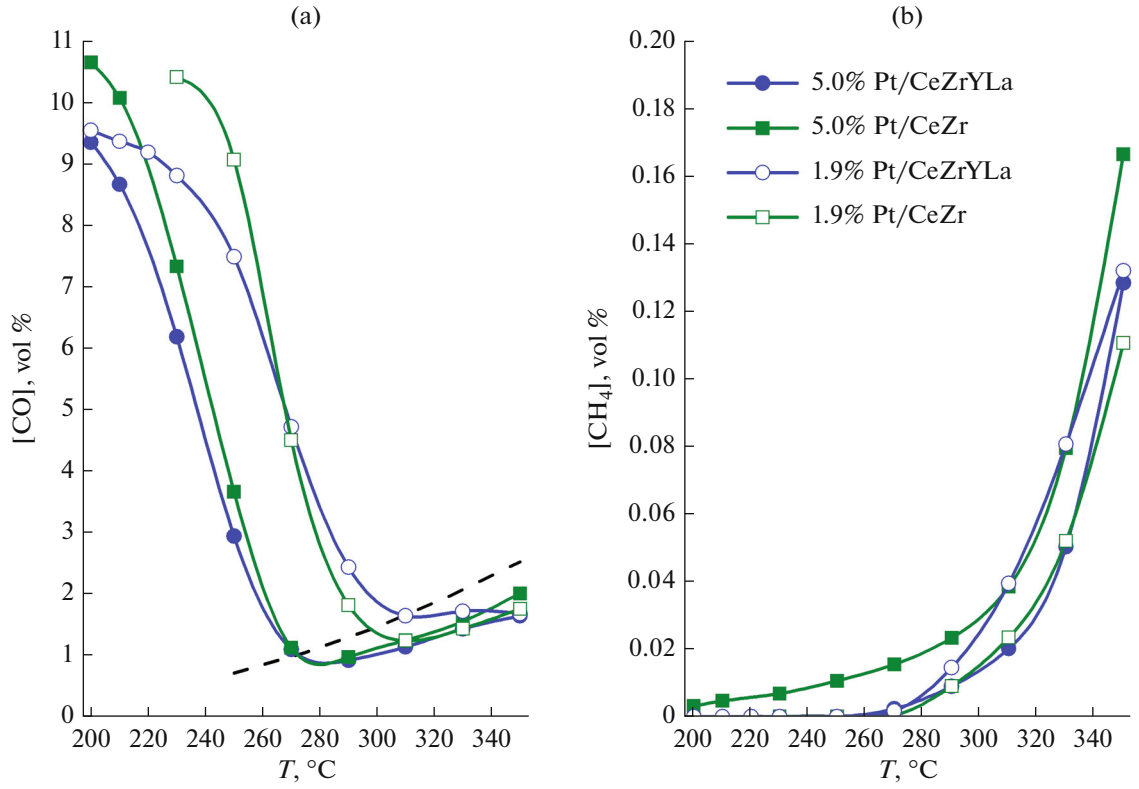

Fig. 1. Temperature dependency of (a) CO and (b) CH_4 concentrations in the outlet gas after WGS. Dashed line—the theoretical equilibrium CO concentration; the composition of the feed gas (vol %): 10 CO, 15 CO_2, 45 H_2, 30 H_2O; WHSV—30000 mL g_{cat}^{-1} h^{-1}.

between the cations determined from the parameter meets the targeted one which indicates homogeneity of the composition of the synthesized oxide. The average size of SCR is $D_{XRD} = 5.0 \pm 0.5$ nm. The CeZrYLa support ($Ce_{0.4}Zr_{0.5}La_{0.05}Y_{0.05}O_2$) represents a mixed oxide with the fluorite-type structure (Fig. 2b). The cell parameter value $a = 5.251(1)$ Å is lower than one for ceria CeO_2 (PDF#00-043-1002, $a = 5.411$ Å) because of the strong cation modification resulting in the formation of a substitution solid solution. The average SCR size is $D_{XRD} = 8.0 \pm 0.5$ nm.

It was shown that both catalysts before and after the catalytic tests contain highly dispersed platinum compounds which cannot be detected by XRD. Comparison of the diffraction patterns of the catalysts and supports (Fig. 2) did not reveal any additional peaks for crystalline Pt-containing phases. For this reason, the samples were later investigated by the atomic pair distribution function method. In the case of the supported catalysts an atomic pair distribution pattern $G(r)$ contains information about interatomic distances in the supported particles, as well as in the support material. To obtain data on the local atomic order in the active phase particles, differential patterns (d–$G(r)$) were calculated by subtracting a normalized pattern of the support from the one of the catalyst (Fig. 3). Based on the analysis of the observed correlations in the arrangement of atoms it was concluded that both the catalysts tested in WGS contain ultra-dispersed particles of metallic platinum Pt^0. Intensive coordination peaks for the distances $r = 2.75$, 4.80, 7.32 Å (Fig. 3) can be distinguished on the differential d–$G(r)$ patterns showing the order of platinum atoms. These interatomic distances are specific for the crystal structure of metallic platinum. The model pattern $G(r)$ calculated for Pt^0 particles is in good agreement with the experimental one. A gradual decrease of amplitude of coordination peaks with an increase of distance on the experimental d–$G(r)$ patterns is associated with the size effect (ultra-small particles). The model $G(r)$ pattern for the Pt^0 particles of 1.5 nm in size matches the experimental d–$G(r)$ ones much better. Therefore, the analysis of the short-range atomic order has shown that the catalysts tested in WGS contain predominantly ultra-dispersed particles of metallic platinum Pt^0. A precision analysis of the particle size by the atomic pair distribution function method is challenging, additional methods should be applied.

The catalysts after the reaction were also studied using TEM and CO chemisorption. For example, Fig. 4 shows the micrographs of the samples of the catalysts containing 5 wt % Pt (the ones for 1.9 wt % Pt

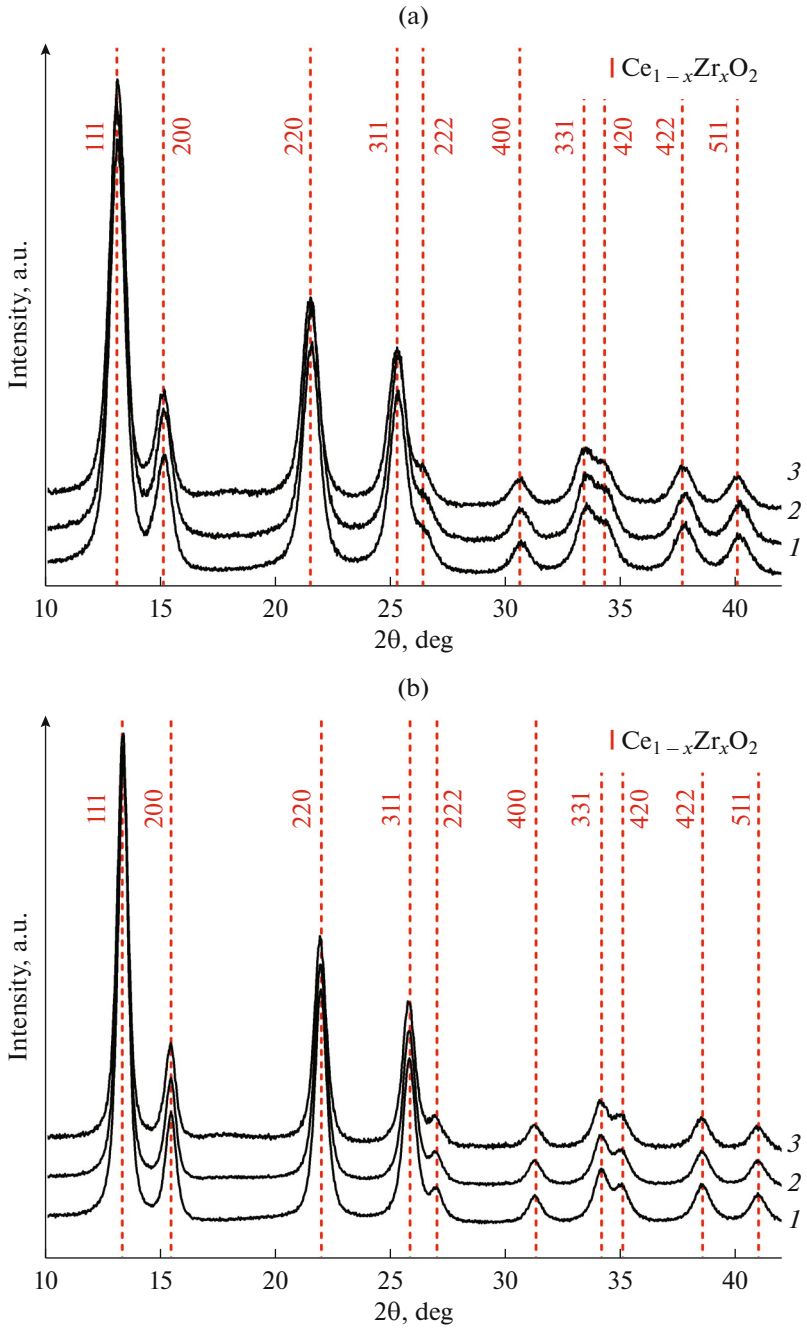

Fig. 2. Diffraction patterns of the supports and the catalysts based on them containing 5 wt % Pt: CeZr (a), CeZrYLa (b); (*1*) the support, (*2*) the catalyst before WGS, (*3*) the catalyst after WGS.

samples are not presented since they are similar). It can be seen that the Pt particles after the reaction have a hemisphere-like shape, retain their high dispersion and are uniformly distributed. These results along with the ones presented earlier in [37, 46] confirm the viability of the sorption-hydrolytic technique for preparation of the catalysts with good reproducibility of the supported metal particle size in them.

It results from the Pt particle size distribution graphs (Fig. 5) based on the TEM data that the average Pt particles size does not exceed 2 nm for all 4 samples. At the same time, it should be noted that in the case of CeZr support it was less than one for CeZrYLa regardless of Pt loading. It can be likely caused by the larger S_{BET} of the CeZr support (Table 1).

Surprisingly, for all 4 samples the average Pt particle size calculated from CO chemisorption data turned out to be 2–3 times larger than ones calculated from the TEM data (Table 2) and pair distribution function method. Given the well-known fact that the metal

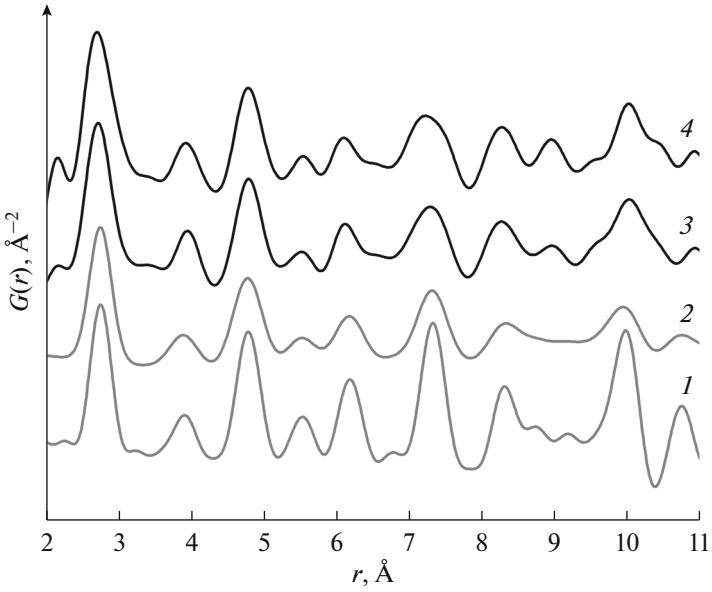

Fig. 3. Differential patterns $d–G(r)$ representing the local atomic order in the catalysts 5% Pt/CeZrYLa (*3*) and 5% Pt/CeZr (*4*) compared to the model patterns $G(r)$ for the metallic Pt^0 particles calculated (*1*) without the particle size taken into account and (*2*) for the particles of 1.5 nm in size.

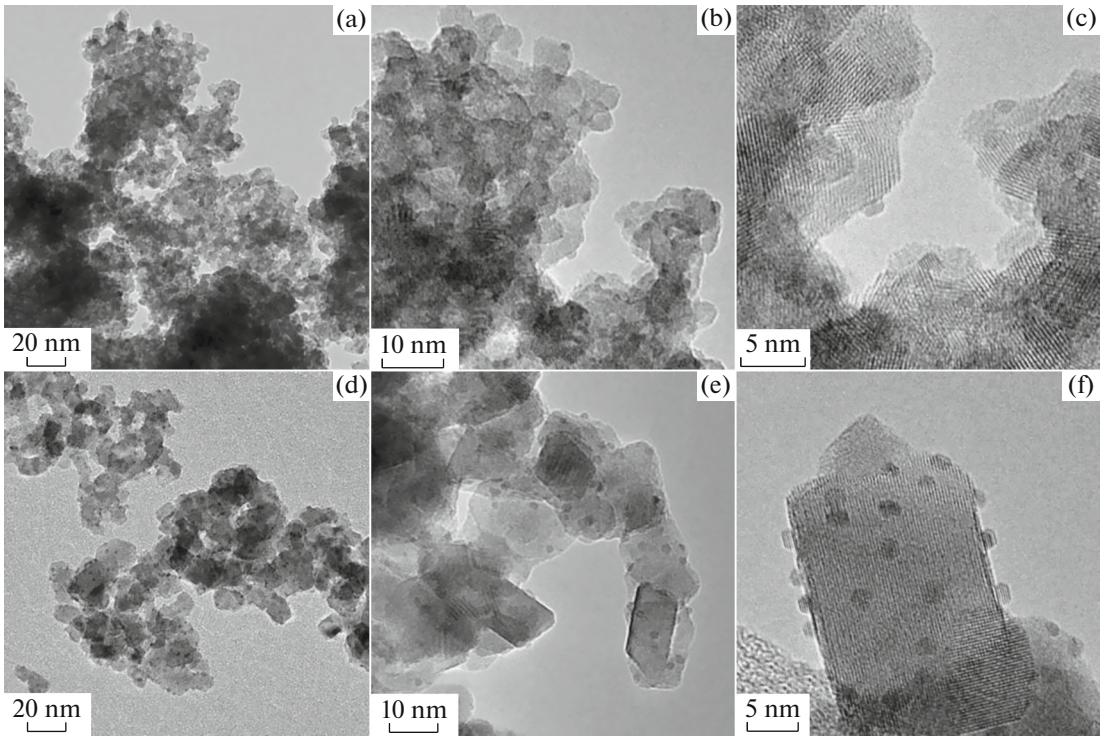

Fig. 4. TEM micrographs of the samples 5% Pt/CeZr (a–c) and 5% Pt/CeZrYLa (d–f) after WGS.

particles can be "decorated" by the support if there is a strong interaction between them, one can suggest that a part of the surface of the Pt particles is inaccessible for CO chemisorption. It should also be borne in mind that the result can be affected by inaccurate correspondence to the real picture of the assumptions used for calculations about the spherical shape of particles and the adsorption of one CO molecule on one Pt atom. It should be noted that after the first chemisorption cycle and treatment with air the next

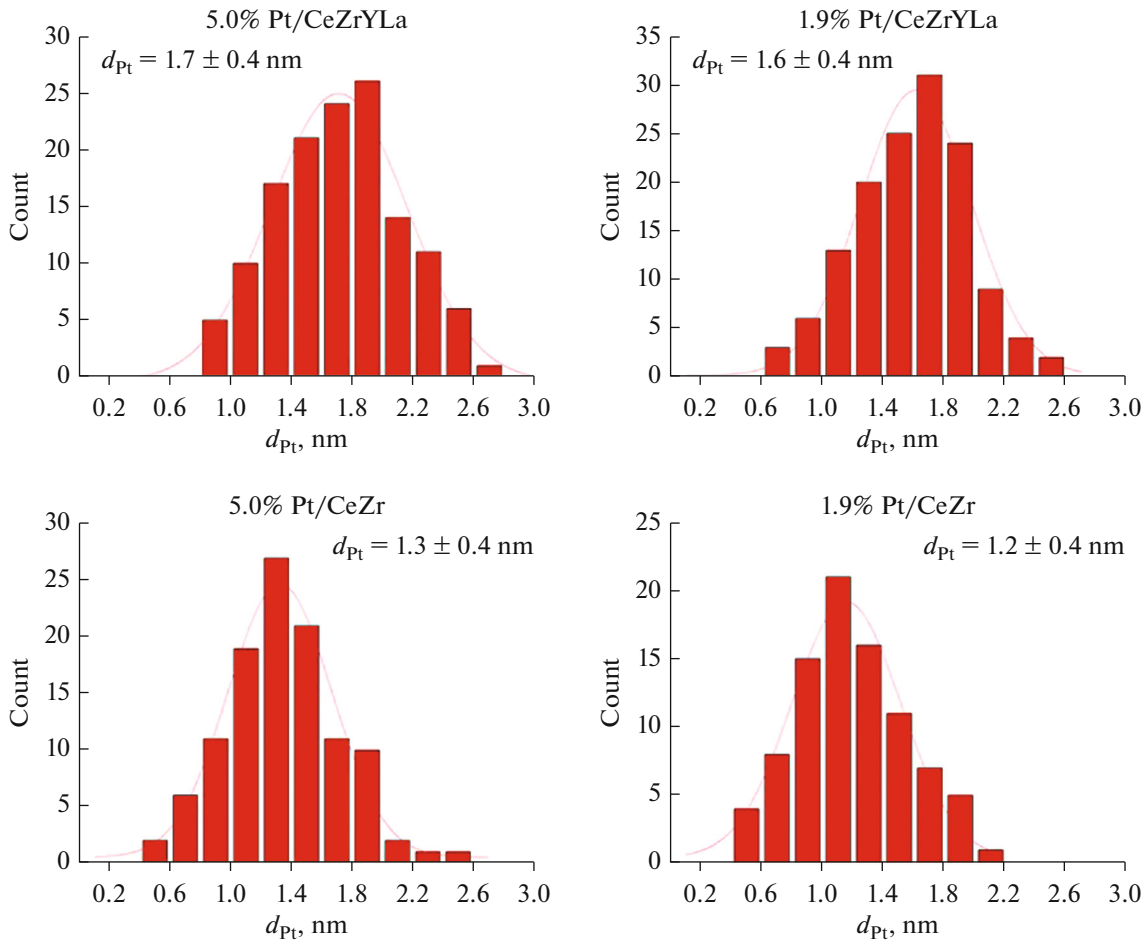

Fig. 5. Pt particle size distributions calculated from TEM data. About 100–130 particles were used to plot every distribution.

measurements resulted in larger values of the specific surface area and, hence, to lower Pt particle size. This difference is particularly noticeable in the case of the catalysts based on CeZrYLa. It is difficult to discuss the causes of the observed phenomenon without any additional investigations; however, one can suppose that after exposure the catalysts to air the Pt particles come out on the surface which leads to an increase of the fraction of the accessible metal surface. In addition, segregation of Pt particles is also known when processed in an oxidizing atmosphere [47].

Unfortunately, it is difficult to calculate turnover frequencies (intrinsic catalytic activity) correctly because of the uncertainty in the CO chemisorption results on the area of the supported platinum accessible surface, for this reason, the influence of the support composition on the reaction rate can only be evaluated indirectly. The calculation of the specific reaction rate per 1 g of Pt for the catalysts containing 5 wt % Pt shows that this parameter is a little higher for the catalyst based on CeZrYLa, compared to the one based on CeZr, at the CO conversion less than 30% (Fig. 6). Taking into account smaller Pt particles in the case of CeZr, it can be concluded that the WGS specific reaction rate per one active site is also higher for the catalysts Pt/CeZrYLa. However, this difference seems to be small, that is why it can be easily compensated by the difference in the specific surface area of

Table 2. Specific surface area and Pt particle size calculated from the CO chemisorption data

Sample	Cycle	S_{Pt}, m^2/g_{cat}	S_{Pt}, m^2/g_{Pt}	d_{Pt}, nm
1.9% Pt/CeZr	1	2.3	121	2.3
	2	3.3	174	1.6
5.0% Pt/CeZr	1	3.3	65	4.3
	2	4.0	81	3.5
1.9% Pt/CeZrYLa	1	1.9	100	2.8
	2	4.1	215	1.3
5.0% Pt/CeZrYLa	1	2.4	49	5.7
	2	3.4	68	4.1

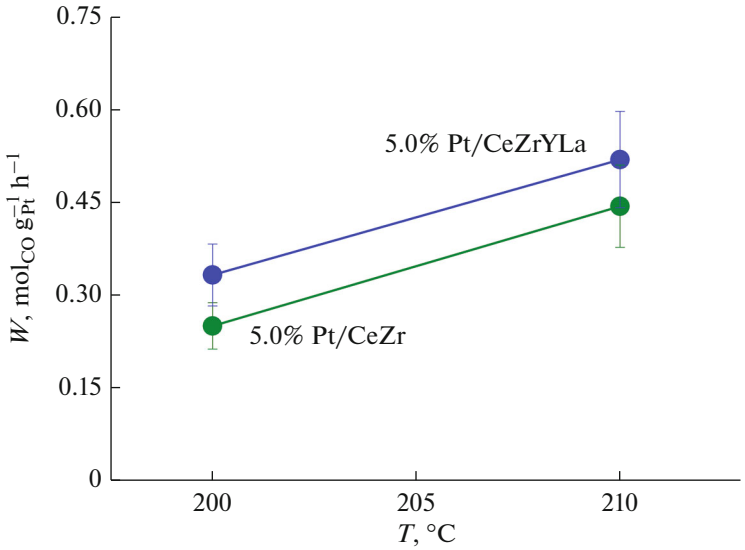

Fig. 6. WGS specific reaction rate per gram of Pt for the catalysts containing 5.0 wt % Pt. The composition of the feed gas (vol.): 10 CO, 15 CO_2, 45 H_2, 30 H_2O; WHSV—30000 mL g_{cat}^{-1} h^{-1}.

the supports leading to similar effectiveness of the catalysts (Fig. 1).

CONCLUSION

A comparative study was made of the structure and catalytic characteristics of the samples *X* wt % Pt/$Ce_{0.75}Zr_{0.25}O_2$ and *X* wt % Pt/$Ce_{0.4}Zr_{0.5}Y_{0.05}La_{0.05}O_2$ (*X* = 1.9, 5.0). It was shown using X-ray diffraction that both the oxide supports represent substitutional solid solutions of cubic structure based on CeO_2 structure. The support $Ce_{0.75}Zr_{0.25}O_2$ has larger specific surface area which is likely the reason of higher dispersion of the supported Pt particles. The results of catalytic tests indicate that, at the same platinum content, the composition of the support does not significantly affect the temperature at which maximum CO conversion is reached, the amount of methane formed as a result of the side reaction, and the reaction rate per gram of Pt. Therefore, one can conclude that the intrinsic catalytic activity calculated per on Pt surface atom may be slightly higher for the samples based on $Ce_{0.4}Zr_{0.5}Y_{0.05}La_{0.05}O_2$; however, it is likely compensated by larger Pt particle size leading to similar effectiveness of the catalysts.

ACKNOWLEDGMENTS

The study of the samples by transmission electron microscopy was carried out using facilities of the shared research center "National center of investigation of catalysts" at Boreskov Institute of Catalysis. The authors also thank the shared research center VTAN NSU for providing access to the measuring equipment.

FUNDING

This work was supported by Russian Science Foundation under the project no. 21-73-20075 (A.M. Gorlova, V.P. Pakharukova, O.A. Stonkus, V.N. Rogozhnikov).

CONFLICT OF INTEREST

The authors declare that they have no conflicts of interest.

REFERENCES

1. Matus, E.V., Nefedova, D.V., Sukhova, O.B., Ismagilov, I.Z., Ushakov, V.A., Yashnik, S.A., Nikitin, A.P., Kerzhentsev, M.A., and Ismagilov, Z.R., *Kinet. Catal.,* 2019, vol. 60, no. 4, p. 496.
2. Sadykov, V.A., Simonov, M.N., Bespalko, Yu.N., Bobrova, L.N., Eremeev, N.F., Arapova, M.V., Smal', E.A., Mezentseva, N.V., and Pavlova, S.N., *Kinet. Catal.,* 2019, vol. 60, no. 5, p. 582.
3. Park, E.D., Lee, D., and Lee, H.C., *Catal. Today,* 2009, vol. 139, no. 4, p. 280.
4. Il'ichev, A.N., Bykhovsky, M.Ya., Fattakhova, Z.T., Shashkin, D.P., Fedorova, Yu.E., Matyshak, V.A., and Korchak, V.N., *Kinet. Catal.,* 2019, vol. 60, no. 5, p. 661.
5. Konishcheva, M.V., Svintsitskiy, D.A., Potemkin, D.I., Rogozhnikov, V.N., Sobyanin, V.A., and Snytnikov, P.V., *ChemistrySelect,* 2020, vol. 5, no. 3, p. 1228.
6. Palma, V., Ruocco, C., Cortese, M., Renda, S., Meloni, E., Festa, G., and Martino, M., *Metals* (Basel), 2020, vol. 10, no. 7, p. 1.
7. Pal, D.B., Chand, R., Upadhyay, S.N., and Mishra, P.K., *Renewable Sustainable Energy Rev.,* 2018, vol. 93, p. 549.
8. LeValley, T.L., Richard, A.R., and Fan, M., *Int. J. Hydrogen Energy,* 2014, vol. 39, no. 30, p. 16983.

9. Gonzalez Castaño, M., Reina, T.R., Ivanova, S., Centeno, M.A., and Odriozola, J.A., *J. Catal.,* 2014, vol. 314, p. 1.
10. Ratnasamy, C. and Wagner, J., *Catal. Rev. Sci. Eng.,* 2009, vol. 51, no. 3, p. 325.
11. Wu, Z., Mann, A.K.P., Li, M., and Overbury S.H., *J. Phys. Chem. C,* 2015, vol. 119, no. 13, p. 7340.
12. González-Castaño, M., Ivanova, S., Ioannides, T., Centeno, M.A., and Odriozola, J.A., *Catal. Sci. Technol.,* 2017, vol. 7, no. 7, p. 1556.
13. Li, Y., Kottwitz, M., Vincent, J.L., Enright, M.J., Liu, Z., Zhang, L., Huang, J., Senanayake, S.D., Yang, W.C.D., Crozier, P.A., Nuzzo, R.G., and Frenkel, A.I., *Nat. Commun.,* 2021, vol. 12, no. 1, p. 1.
14. Meira, D.M., Ribeiro, R.U., Mathon, O., Pascarelli, S., Bueno, J.M.C., and Zanchet, D., *Appl. Catal. B: Environ.,* 2016, vol. 197, p. 73.
15. Yuan, K., Guo, Y., Lin, Q.L., Huang, L., Ren, J.T., Liu, H.C., Yan, C.H., and Zhang, Y.W., *J. Catal.,* 2021, vol. 394, p. 121.
16. Lee, K.J., Kim, Y., Lee, J.H., Cho, S.J., Kwak, J.H., and Moon, H.R., *Chem. Mater.,* 2017, vol. 29, no. 7, p. 2874.
17. Devaiah, D., Reddy, L.H., Park, S.E., and Reddy, B.M., *Catal. Rev. Sci. Eng.,* 2018, vol. 60, no. 2, p. 177.
18. Mamontov, E., Egami, T., Brezny, R., Koranne, M., and Tyagi, S., *J. Phys. Chem. B,* vol. 104, no. 47, p. 11110.
19. Li, J., Liu, X., Zhan, W., Guo, Y., Guo, Y., and Lu, G., *Catal. Sci. Technol.,* 2016, vol. 6, no. 3, p. 897.
20. Song, L., Zhu, L., and Li, L., *Crystals,* 2018, vol. 8, p. 261.
21. Deshpande, P.A., Hegde, M.S., and Madras, G., *Appl. Catal. B: Environ.,* 2010, vol. 96, nos. 1–2, p. 83.
22. Ricote, S., Jacobs, G., Milling, M., Ji, Y., Patterson, P.M., and Davis, B.H., *Appl. Catal. A: Gen.,* 2006, vol. 303, no. 1, p. 35.
23. Lee, K., Knoblauch, N., Agrafiotis, C., Pein, M., Roeb, M., and Sattler, C., *Open Ceram.,* 2022, vol. 10, p. 100269.
24. Yuan, K., Sun, X.C., Yin, H.J., Zhou, L., Liu, H.C., Yan, C.H., and Zhang, Y.W., *J. Energy Chem.,* 2022, vol. 67, p. 241.
25. Li, S., Deng, J., Wang, J., Chen, Y., and Li, Y., *J. Rare Earths,* 2022. https://doi.org/10.1016/j.jre.2022.11.009
26. Duarte de Farias, A.M., Nguyen-Thanh, D., and Fraga, M.A., *Appl. Catal. B: Environ.,* 2010, vol. 93, nos. 3–4, p. 250.
27. Sartoretti, E., Novara, C., Chiodoni, A., Giorgis, F., Piumetti, M., Bensaid, S., Russo, N., and Fino, D., *Catal. Today,* 2022, vols. 390–391, p. 117.
28. Andreeva, D., Idakiev, V., Tabakova, T., Ilieva, L., Falaras, P., Bourlinos, A., and Travlos, A., *Catal. Today,* 2002, vol. 72, nos. 1–2, p. 51.
29. Tabakova, T., Ilieva, L., Ivanov, I., Manzoli, M., Zanella, R., Petrova, P., and Kaszkur, Z., *J. Rare Earths,* 2019, vol. 37, no. 4, p. 383.
30. Andreeva, D., Ivanov, I., Ilieva, L., Abrashev, M.V., Zanella, R., Sobczak, J.W., Lisowski, W., Kantcheva, M., Avdeev, G., and Petrov, K., *Appl. Catal. A: Gen.,* 2009, vol. 357, no. 2, p. 159.
31. Kaur, T., Singh, K., and Kolte, J., *Mater. Today Proc.,* 2022. https://doi.org/10.1016/j.matpr.2022.11.331
32. Chanapattharapol, K.C., Krachuamram, S., Kidkhunthod, P., and Poo-arporn, Y., *Solid State Sci.,* 2020, vol. 99, p. 106066.
33. Ballauri, S., Sartoretti, E., Hu, M., D'Agostino, C., Ge, Z., Wu, L., Novara, C., Giorgis, F., Piumetti, M., Fino, D., Russo, N., and Bensaid, S., *Appl. Catal. B: Environ.,* 2023, vol. 320, p. 121898.
34. Shi, J., Li, H., Genest, A., Zhao, W., Qi, P., Wang, T., and Rupprechter, G., *Appl. Catal. B: Environ.,* 2022, vol. 301, p. 120789.
35. Poggio-Fraccari, E., Mariño, F., Laborde, M., and Baronetti, G., *Appl. Catal. A: Gen.,* 2013, vols. 460–461, no. 3, p. 15.
36. Shoynkhorova, T.B., Simonov, P.A., Potemkin, D.I., Snytnikov, P.V., Belyaev, V.D., Ishchenko, A.V., Svintsitskiy, D.A., and Sobyanin, V.A., *Appl. Catal. B: Environ.,* 2018, vol. 237, p. 237.
37. Gorlova, A.M., Panafidin, M.A., Shilov, V.A., Pakharukova, V.P., Snytnikov, P.V., and Potemkin, D.I., *Int. J. Hydrogen Energy,* 2023, vol. 48, no. 32, p. 12015.
38. Egami, T. and Billinge, S.J.L., *Underneath the Bragg Peaks*, Pergamon Materials Series, Amsterdam: Elsevier, 2012.
39. Pakharukova, V.P., Moroz, É.M., and Zyuzin, D.A., *J. Struct. Chem.,* 2010, vol. 51, no. 2, p. 274.
40. Moroz, E.M., Pakharukova, V.P., and Shmakov, A.N., *Nucl. Instrum. Methods Phys. Res. Sect. A. Accel. Spectrom. Detect. Assoc. Equip.,* vol. 603, nos. 1–2, p. 99.
41. Qiu, X., Thompson, J.W., and Billinge, S.J.L., *J. Appl. Crystallogr.,* 2004, vol. 37, no. 4, p. 678.
42. Farrow, C.L., Juhas, P., Liu, J.W., Bryndin, D., Božin, E.S., Bloch, J., Proffen, T., and Billinge, S.J.L., *J. Phys. Condens. Matter,* 2007, vol. 19, no. 33, p. 335219.
43. *Inorganic Crystal Structure Database (ICSD-for-WWW),* Karlsruhe: Fachinformationszentrum (FIZ), 2007.
44. Masadeh, A.S., Božin, E.S., Farrow, C.L., Paglia, G., Juhas, P., Billinge, S.J.L., Karkamkar, A., and Kanatzidis, M.G., *Phys. Rev.,* vol. 76, no. 11, p. 115413.
45. Kunwar, D. and Zhou, S., DeLaRiva, A., Peterson, E.J., Xiong, H., Isidro Pereira-Hernández, X., Purdy, S.C., ter Veen, R., H. Brongersma, H., Miller, J.T., Hashiguchi, H., Kovarik, L., Lin, S., Guo, H., Wang, Y., and Datye, A.K., *ACS Catal.,* 2019, vol. 9, no. 5, p. 3978.